2.14   AN INTERCOMPARISON OF BULK AERODYNAMIC ALGORITHMS OVER SEA ICE DURING THE SURFACE HEAT BUDGET OF THE ARCTIC OCEAN EXPERIMENT

Michael A. Brunke[*], Mingyu Zhou[**], Xubin Zeng
Department of Atmospheric Sciences, The University of Arizona, Tucson, AZ
[**]Also National Research Center for Marine Environmental Forecasts, Beijing, China

Edgar L. Andreas
U.S. Army Cold Regions Research and Engineering Laboratory, Hanover, NH

1. INTRODUCTION

The polar regions are a very important part of the global climate, as they are a sink for the energy created in the Tropics. An integral component of the polar system is sea ice. Its presence transforms the exchange of energy between the atmosphere and the ocean. Sea ice also effects climate more generally through the ice-snow albedo feedback mechanism (Curry et al. 1995) and through the oceanic feedbacks involving ice growth and melt and the freshwater balance at the ice-ocean interface (Stocker et al. 2001). Several global models have simulated under increased-CO_2 scenarios that warming is greatest in the Arctic enhanced by the retreat and thinning of the sea ice (Randall et al. 1998, Houghton et al. 1990). These models show large differences between the warming of the temperatures in this region (Houghton et al. 1990, Gates et al. 1996). These models are even problematic in their control simulations in this region. For instance, the newest version of the National Center for Atmospheric Research (NCAR) Community Climate System Model (CCSM) is too warm by 8 K in the polar regions and has sea ice that is too thin in the Arctic (Kiehl and Gent 2004).

These problems could be partially due to their parameterizations of the surface energy balance. Small changes in this have been shown to effect model ice thickness (Bitz and Lipscomb 1999). The net surface energy flux

$$F_{net} = R_{SW} + R_{LW} - H_s - H_l + G \qquad (1)$$

includes the net shortwave (SW) radiative flux (R_{SW}), the net longwave (LW) radiative flux (R_{LW}), the conductive heat flux from the interior of the ice and snow (G), and the surface turbulent fluxes of heat (sensible heat or SH flux, H_s) and moisture

(latent heat or LH flux, H_l). In modeling, these turbulent fluxes along with momentum flux or wind stress τ are calculated using bulk aerodynamic algorithms. These algorithms generally employ Monin-Obukhov similarity theory to derive these fluxes from bulk variables such as wind speed, temperature, and humidity. This study intercompares with fluxes observed during the Surface Heat Budget of the Arctic Ocean (SHEBA) experiment four such algorithms that are used in climate and numerical weather prediction models: version 2 of the CCSM, the European Centre for Medium-Range Weather Forecasts (ECMWF) model, the Arctic Regional Climate System Model (ARCSyM), and the National Center for Environmental Prediction (NCEP) Global Forecasting System (GFS) model.

TABLE 1. The formulation of the roughness lengths or exchange coefficients for the four algorithms compared in this study.

Algor-ithm	Roughness lengths or exchange coefficients
CCSM	$z_{om} = z_{ot} = z_{oq} = 0.0005$ m
ECMWF	$z_{om} = z_{ot} = z_{oq} = 0.001$ m
ARCSyM	$z_{om} = 0.04$ m if $d_s < 0.005$ m and $z_{om} = 0.06$ m if $d_s > 0.005$ m[a]; $C_q = 1.0022 \times 10^{-3} + 8.22 \times 10^{-5} \Delta T + 2.66 \times 10^{-4} U,$ $C_t = 0.94 C_q$
GFS	$z_{om} = z_{ot} = z_{oq} = 0.0001$ m

[a] d_s is snow depth.

*   *Corresponding author address:* Michael A. Brunke, Department of Atmospheric Sciences, The University of Arizona, 1118 E. 4th St., PO Box 210081, Tucson, AZ 85721; e-mail: brunke@atmo.arizona.edu

TABLE 2. The stability terms used in the four algorithms compared in this study.

Algorithm	Stability terms
CCSM	$\psi_m = 2\ln(\frac{1+x}{2}) + \ln(\frac{1+x^2}{2}) - 2\arctan x + \frac{\pi}{2}$ and $\psi_t = 2\ln(\frac{1+x^2}{2})$ where $x = [1 - 16(\frac{z}{L})]^{1/4}$ if $z/L < 0$; $\psi_m = \psi_t = -5(z/L)$ if $z/L > 0$
ECMWF	Same as in CCSM if $z/L < 0$; $\psi_m = \psi_t = -0.7(\frac{z}{L}) - [0.75(\frac{z}{L}) - 10.72]e^{-0.35(z/L)}$ if $0 \le z/L \le 200$; $\psi_m = \psi_t = -0.7(\frac{z}{L}) - 10.72$ if $z/L > 200$
ARCSyM	$f_m = \dfrac{1 - 40\,Ri_b}{1 + C_{m1}\,Ri_b^{1/2}}$ where $C_{m1} = 296\,C_{mn}(\frac{z}{z_{om}})^{1/2}$ if $Ri_b < 0$; $f_m = \dfrac{1}{(1 + 20\,Ri_b)^2}$ if $Ri_b > 0$
GFS	$\psi_m = \dfrac{[-3.975 + 12.32(\frac{z}{L})]\frac{z}{L}}{1 - 7.755(\frac{z}{L}) + 6.041(\frac{z}{L})^2}$ and $\psi_t = \dfrac{[-7.941 + 24.75(\frac{z}{L})]\frac{z}{L}}{1 - 8.705(\frac{z}{L}) + 7.899(\frac{z}{L})^2}$ if $\theta_{va} - \theta_{vs} < 0$ K and $z/L > -0.5$; $\psi_m = \ln(\frac{z}{L}) + 2(\frac{z}{L})^{-1/4} - 0.8776$ and $\psi_t = \ln(\frac{z}{L}) + 0.5(\frac{z}{L})^{-1/2} + 1.386$ if $\theta_{va} - \theta_{vs} < 0$ K and $z/L < -0.5$; $\psi_m = A_o - A + \ln(\frac{A+1}{A_o+1})$ and $\psi_t = B_o - B + \ln(\frac{B+1}{B_o+1})$ where $A = [1 + 20(z/L)]^{1/2}$, $A_o = [1 + 20(z_{om}/L)]^{1/2}$, $B = [1 + 20(z/L)]^{1/2}$, and $B_o = [1 + 20(z_{ot}/L)]^{1/2}$ if $\theta_{va} - \theta_{vs} \ge 0$ K

[a] In ARCSyM, $C_m = C_{mn} f_m$ where $C_{mn} = k^2 / [\ln(z/z_{om})]^2$.
[b] Ri_b is the bulk Richardson number (see Eq. (8)).

2. BULK AERODYNAMIC ALGORITHMS

In general, bulk aerodynamic algorithms such as the four being compared in this study calculate the turbulent fluxes thusly:

$$\tau = \rho_a C_m U^2 \tag{2}$$

$$H_s = \rho_a c_p C_t U(\theta_s - \theta_a) \tag{3}$$
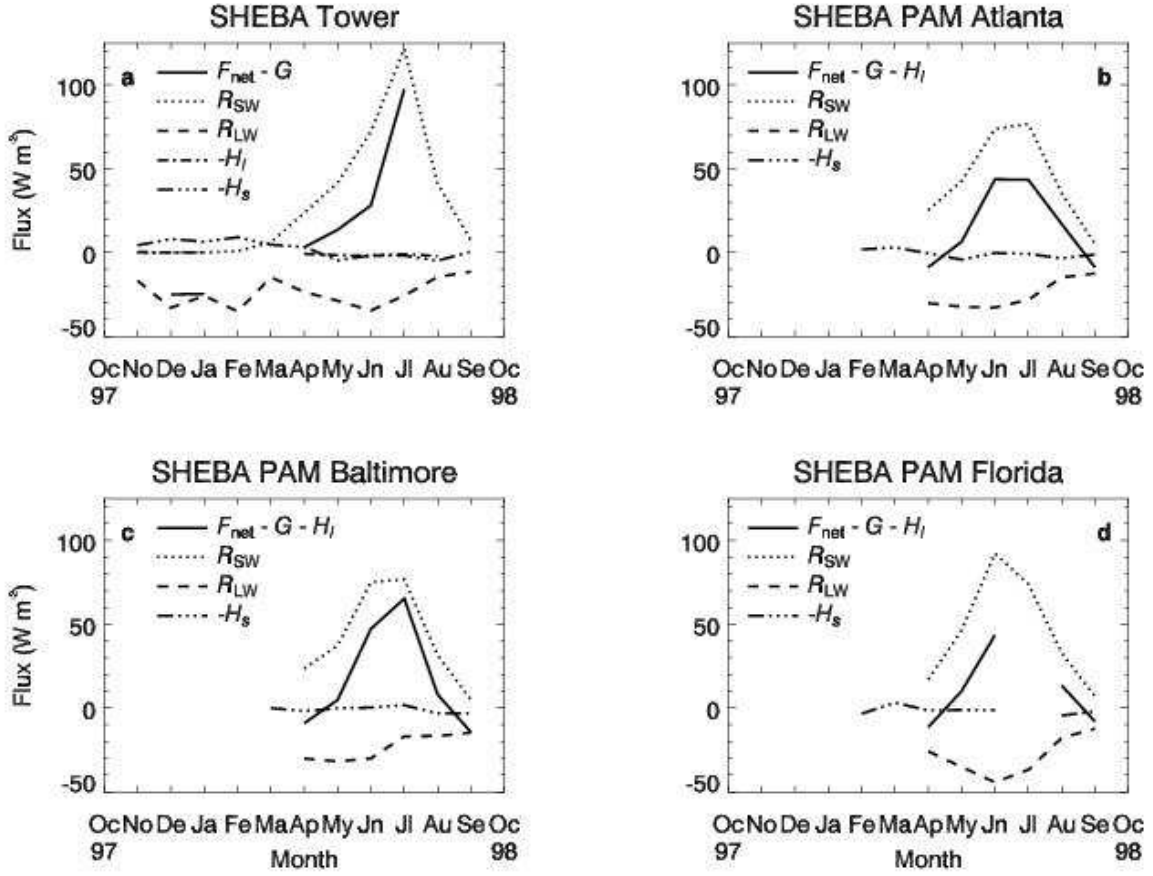
$$H_l = \rho_a L_s C_q U(q_s - q_a) \tag{4}$$

FIG. 1. The energy budget at each of the sites looked at in this study: (a) the 20-m tower and the PAM stations (b) Atlanta, (c) Baltimore, and (d) Florida. At the tower, the net shortwave radiation (dotted line), net longwave radiation (dashed line), latent heat flux (dot-dash line), sensible heat flux (triple dot-dash line), and the net sum of those fluxes (solid line) are shown. At the PAM stations, only the net shortwave radiation (dotted line), net longwave radiation (dashed line), sensible heat flux (triple dot-dash line), and the net sum of those fluxes (solid line) are shown, since latent heat flux was not measured at these sites. Positive fluxes are downward into the ice.

where ρ_a is the density of air, c_p is the heat capacity of air at constant pressure, L_s is the latent heat of sublimation, U is wind speed, θ_s and θ_a are the potential temperature at the surface and first model level respectively, q_s and q_a are the specific humidity at the surface and first model level respectively, and C_m, C_t, and C_q are the turbulent exchange coefficients for momentum, heat, and moisture respectively. Generally, these exchange coefficients are formulated as a function of roughness lengths z_{om}, z_{ot}, and z_{oq} for momentum, heat, and moisture respectively:

$$C_m = \frac{k^2}{[\ln(\frac{z}{z_{om}}) - \psi_m]^2} \tag{5}$$

$$C_t = \frac{k^2}{[\ln(\frac{z}{z_{om}}) - \psi_m][\ln(\frac{z}{z_{ot}}) - \psi_t]} \tag{6}$$

$$C_q = \frac{k^2}{[\ln(\frac{z}{z_{om}}) - \psi_m][\ln(\frac{z}{z_{oq}}) - \psi_t]} \tag{7}$$

where k is the von Kármán constant and z is the height of the first model layer. The terms ψ_m and ψ_t are parameters for momentum and heat/moisture respectively added to take into account the effects of stability. Generally, these are a function of z / L, L being the characteristic
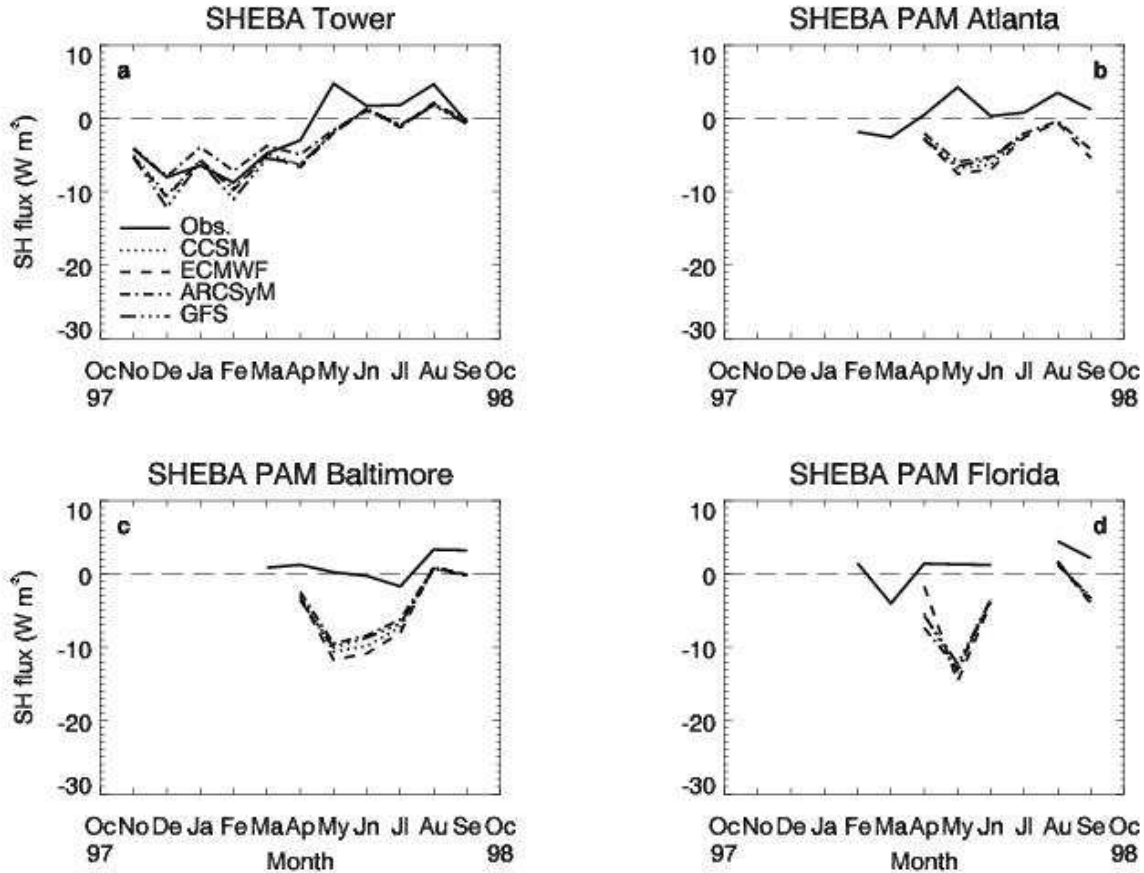
FIG. 2. Monthly mean observed covariance sensible heat fluxes (solid lines) along with the algorithm-produced fluxes from CCSM (dotted lines), ECMWF (dashed lines), ARCSyM (dot-dash lines), and GFS (triple dot-dash lines) at (a) the 20-m tower and the PAM stations (b) Atlanta, (c) Baltimore, and (d) Florida.

Obukhov length which is equal to $u_*^2\theta_v / kg\theta_{v*}$[1], and z_{om}, z_{ot}, and z_{oq} are considered to be constant and equal to each other. The four algorithms differ by how the roughness lengths and the terms ψ_m and ψ_t are formulated. These differences are explained in Tables 1 and 2.

3. DATA

The data used in this study was from the SHEBA experiment undertaken on an ice floe in the Arctic Ocean north of Alaska from October 1997 to October 1998. Turbulent flux measurements were made at a 20-m high tower that was located at the ice camp and at four

portable mesonet (PAM) stations surrounding the ice camp. On the tower, temperature/relative humidity sensors and sonic anemometers were placed at five levels (level 1 at a mean height of 2.2 m, level 2 at 3.2 m, level 3 at 5.1 m, level 4 at 8.9 m, and level 5 split between 13.8 and 17.6 m), and a fast hygrometer was placed at only one level (mean height of 8.1 m). Nearby were radiometric instruments measuring the radiative fluxes and the surface temperature as well as a barometer (Persson et al. 2002). The PAM stations were equipped with temperature/relative humidity sensors, sonic anemometers, radiometers, and barometers (http://www.atd.ucar.edu/rtf/projects/sheba). One of these stations had to be moved several times due to endangerment of being destroyed and thus does not have a continuous record. Data from this station have been excluded from this study.

The direct covariance fluxes measured by the sonic anemometers and the fast hygrometer as

---

1 u_* is the friction velocity, θ_v is the virtual potential temperature, g is the acceleration due to gravity, and θ_{v*} is the scaling parameter for virtual potential temperature = $\overline{(w'\theta_v')}$ / u_* (Garrett 1992).

SHEBA Tower

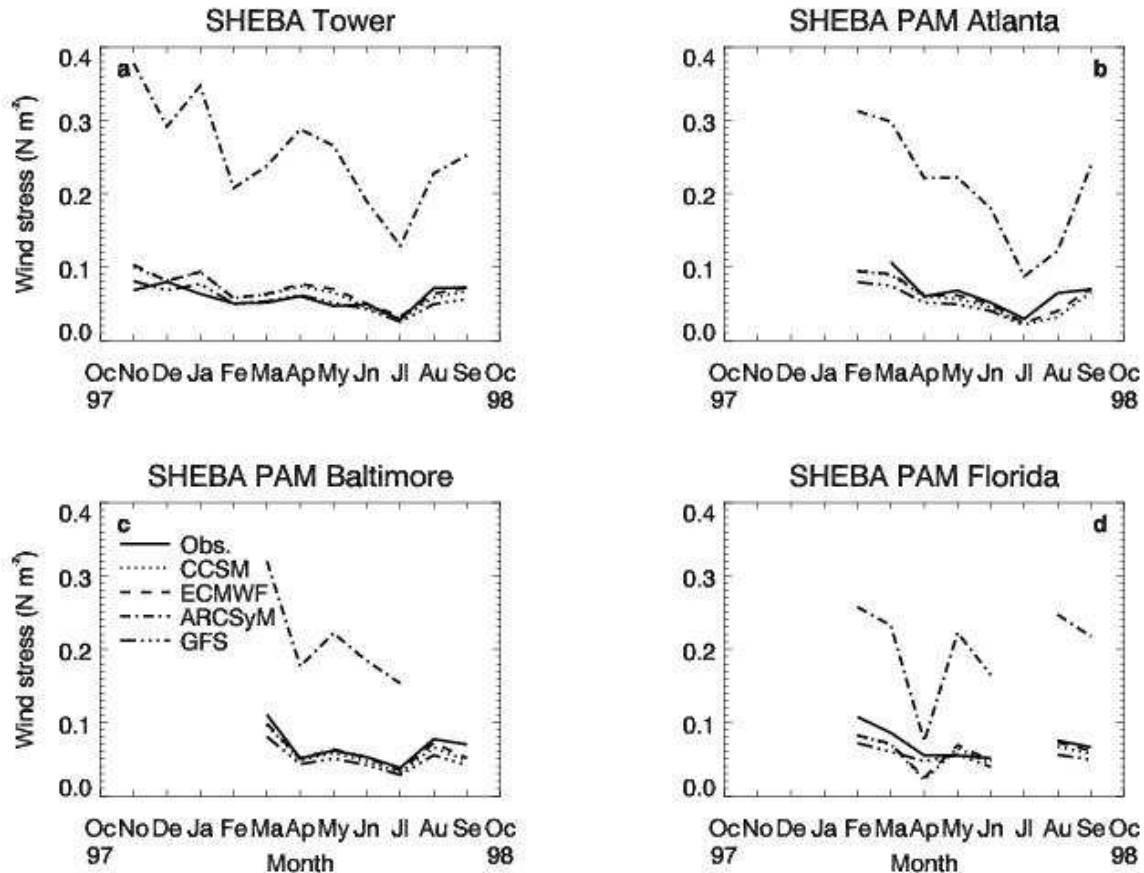SHEBA PAM Atlanta

SHEBA PAM Baltimore

SHEBA PAM Florida

Fig. 3. Same as in Fig. 2 except for wind stress.

well as the meteorological and radiometric measurements were averaged for every hour that there were valuable data which included times when the tower or boom structure was not upwind from the sonic anemometers. Also at the PAM stations, we additionally eliminated the covariance fluxes before the installation of heaters on the sonic anemometers in mid-February and of the surface temperatures derived form the radiometric measurements before the successful installation of heaters on the domes that protected the radiometers. These heaters removed the rime that built up on these instruments which degraded the integrity of the data before the installation of the heaters.

Fig. 1 shows the monthly means of the turbulent and radiative fluxes along with the net sum of these at the four sites looked at in this study. Note that positive fluxes are downward into the ice. The turbulent fluxes (SH flux, triple dot-dash lines, and LH flux, dot-dash lines at the tower only) are small (generally less than ±10 W m^{-2}) compared to the radiative fluxes (net SW flux, dotted lines, and net LW flux, dashed lines).

Thus, the net fluxes (solid lines) are dominated by the LW flux in the winter and the SW flux in the summer.

4. INTERCOMPARISON OF MODEL FLUXES WITH OBSERVED FLUXES
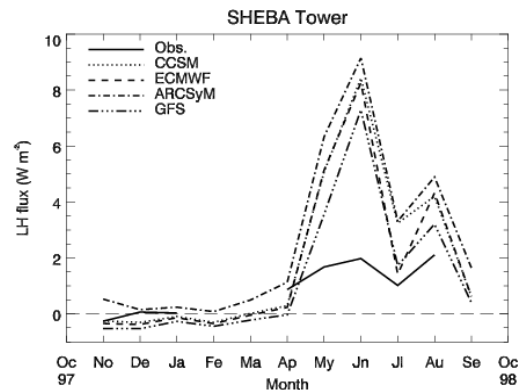
The four bulk aerodynamic algorithms

SHEBA Tower

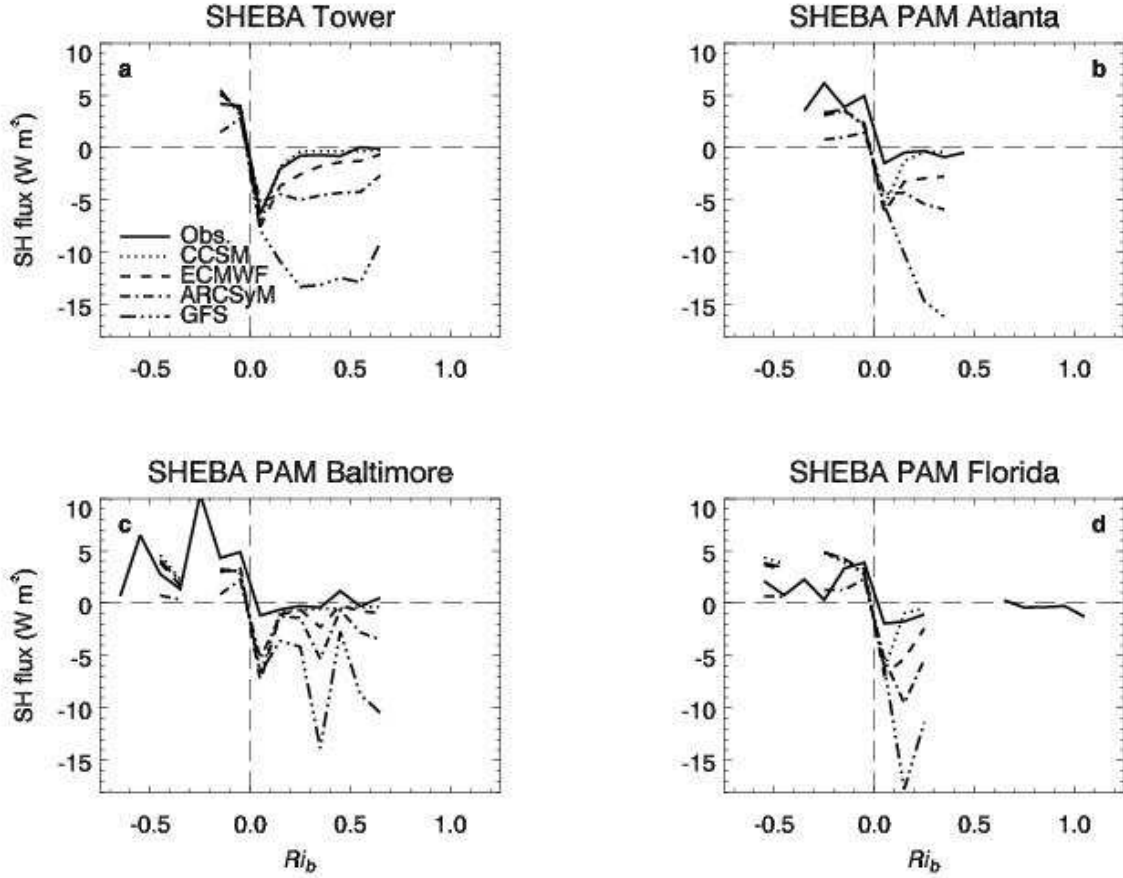Fig. 4. Same as in Fig. 2 except for latent heat flux at the tower only.

FIG. 5. Median observed covariance sensible heat fluxes (solid lines) and the algorithm-produced fluxes from CCSM (dotted lines), ECMWF (dashed lines), ARCSyM (dot-dash lines), and GFS (triple dot-dash lines) as a function of the bulk Richardson number in 0.1 bins at (a) the 20-m tower and the PAM stations (b) Atlanta, (c) Baltimore, and (d) Florida.

their respective models. Then, these algorithms have been run using the observed meteorological measurements of air and surface temperature, wind speed, and relative humidity taken during the SHEBA experiment at the four sites used in this study: the 20-m tower and the PAM stations Atlanta, Baltimore, and Florida.

4.1 Monthly fluxes

Figs. 2-4 compare the monthly mean observed fluxes from these locations as well as those computed by the four algorithms compared in this study.

Observed SH fluxes (Fig. 2) are generally negative during the winter and slightly positive in summer. At the tower (Fig. 2a), the algorithm SH fluxes are quite close to observed in winter. In summer, the algorithm SH fluxes are underestimated at all of the sites.

Observed monthly mean wind stresses (Fig. 3) at all of the sites is relatively constant

throughout the year. The CCSM, ECMWF, and GFS algorithms produce wind stresses that are close to observed, while ARCSyM produces stresses that are much higher than observed.

Observed LH flux (Fig. 4) at the tower is small: near-zero in the winter and less than 2 W m^{-2} in summer. Every algorithm except ARCSyM produces sllightly negative LH fluxes in winter, while all algorithms significantly overestimate LH flux in summer.

4.2 Stability regimes

Figs. 5-7 present the median observed and algorithm fluxes binned as a function of the bulk Richardson number:

$$Ri_b = \frac{gz\,(\theta_{va} - \theta_{vs})}{\theta_{va}\,U^2} \,. \qquad (8)$$

Here Ri_b is defined at 2.5 m.

Observed SH flux (Fig. 5) is positive for

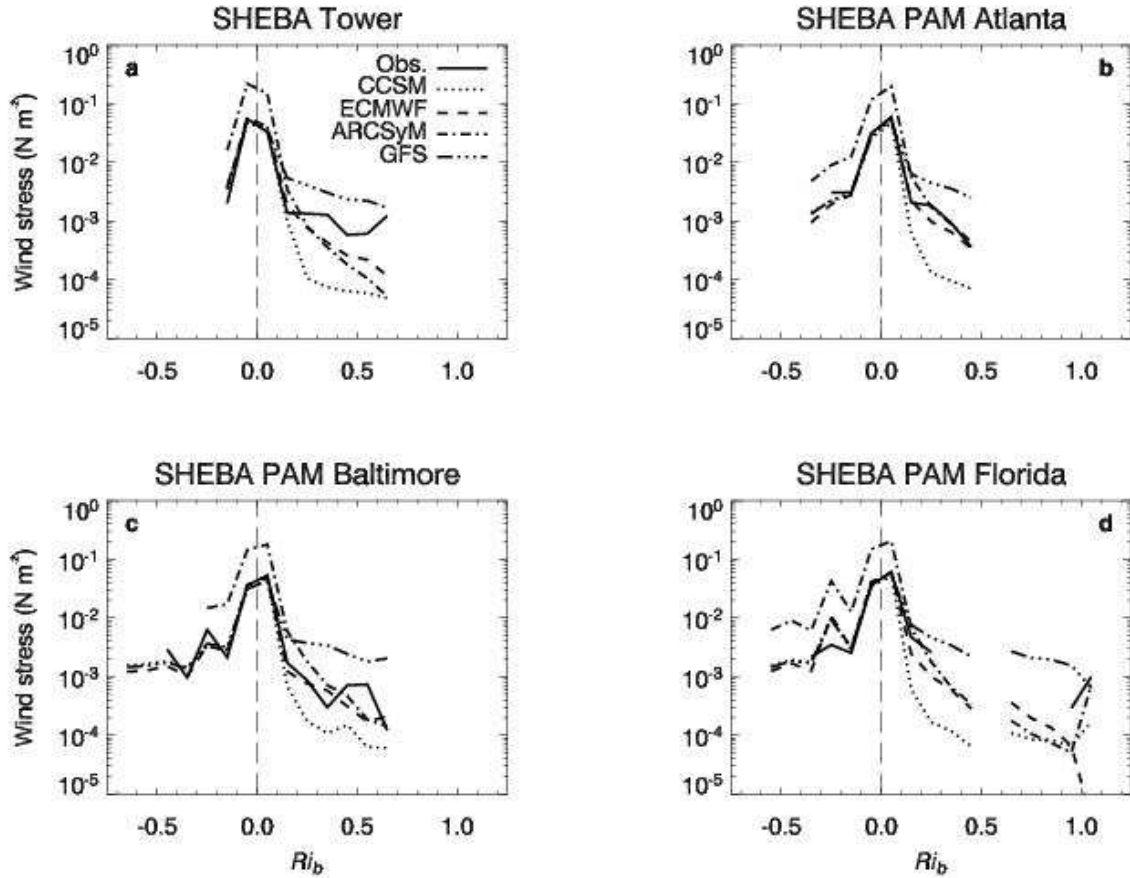FIG. 6. Same as in Fig. 5 except for wind stress.

unstable conditions ($Ri_b < 0$) and generally negative under stable conditions ($Ri_b > 0$). At all locations, there is a minimum in observed SH flux at $Ri_b \approx 0.05$. At more significant stabilities, observed SH flux increases to near-zero values for $Ri_b > 0.1$. This is consistent with previous work (e.g., Mahrt et al. 1998 and Mahrt 1999).

At the tower, all of the algorithms portray the observed minimum very well, but at higher stability only CCSM agrees well with observations. In particular, GFS' SH fluxes are very much underestimated having a minimum under very stable conditions. For unstable conditions, ARCSyM generally underestimates SH flux except at Florida for weakly unstable conditions.

Observed wind stress (Fig. 6) has a maximum under near-neutral conditions with stress under stable ($Ri_b > 0$) and unstable ($Ri_b < 0$) conditions one to two orders of magnitude lower. Under unstable conditions ($Ri_b < 0$), ARCSyM overestimates wind stress. For stable conditions ($Ri_b > 0$), GFS overestimates wind stress while CCSM underestimates wind stress.

At the tower, observed LH flux (Fig. 7) has a maximum of about 1.8 W m^{-2} at $Ri_b \approx -0.05$. With increasing stability, observed LH flux decreases to near-zero for stable conditions ($Ri_b > 0$). Every algorithm except ARCSyM produces LH fluxes similar in nature to their SH fluxes. In ARCSyM LH flux is set to 0 W m^{-2} if the specific humidity difference is negative.
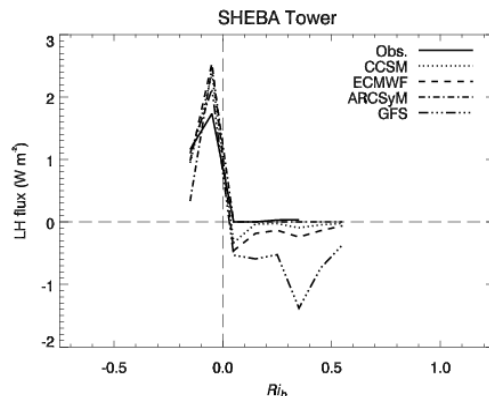

FIG. 7. Same as in Fig. 5 except for latent heat flux at the tower only.

TABLE 3. The median sensible heat fluxes observed and from the four algorithms compared in this study (CCSM, ECMWF, ARCSyM, and GFS) during winter (October to March) at level 1 of the tower and the median differences at the upper levels between the SH flux at the level and the flux at the lowest level relative to the median flux at level 1.

Level	No. obs.		Obs.	CCSM	ECMWF	ARCSyM	GFS
		$Ri_b \leq 0$ (unstable regime)					
1	416	Median	2.55	4.21	4.28	3.01	3.59
2	427	Median difference	+74%	-7%	-9%	+9%	-7%
3	330	Median difference	+59%	-11%	-14%	+29%	-11%
4	421	Median difference	+43%	-11%	-14%	+68%	-10%
5a	405	Median difference	+43%	-14%	-20%	+95%	-14%
5b							
		$0 < Ri_b \leq 0.05$ (weakly stable regime)					
1	1311	Median	-9.60	-10.04	-10.16	-6.70	-10.65
2	1293	Median difference	+11%	-2%	-1%	-19%	-3%
3	856	Median difference	+21%	-3%	+3%	-40%	-1%
4	1217	Median difference	+29%	+7%	+5%	-83%	-2%
5a	1156	Median difference	+31%	+10%	+4%	-116%	-6%
5b							
		$0.05 < Ri_b \leq 0.25$ (transitional regime)					
1	204	Median	-4.45	-3.95	-5.39	-4.79	-11.57
2	203	Median difference	+9%	+3%	-3%	-41%	-7%
3	101	Median difference	+38%	+21%	-9%	-122%	-27%
4	187	Median difference	+72%	+37%	-12%	-257%	-33%
5a	174	Median difference	+63%	+62%	-14%	-385%	-49%
5b							
		$Ri_b > 0.25$ (very stable regime)					
1	44	Median	-0.70	-0.32	-1.55	-4.33	-12.20
2	46	Median difference	+86%	-25%	-19%	-39%	-5%
3	14	Median difference	+79%	-84%	-21%	-118%	-4%
4	30	Median difference	+136%	-141%	-79%	-241%	-11%
5a	28	Median difference	+43%	-241%	-54%	-397%	+3%
5b							

Previous studies have shown that SH flux should decrease in magnitude (become less negative) with increasing height under stable conditions (e.g., Fig. 4 in Howell and Sun 1999). Table 3 lists the median observed SH fluxes at the lowest level of the tower and the median difference between the fluxes at the upper levels and that at the lowest level relative to the median flux at the lowest level for four stability regimes during winter (October to March): $Ri_b \leq 0$ (unstable conditions), $0 < Ri_b \leq 0.05$ (weakly stable conditions), $0.05 <$ $Ri_b \leq 0.25$ (transitional regime), and $Ri_b > 0.25$ (very stable conditions). Under unstable conditions ($Ri_b \leq 0$), the median differences are positive and decrease with height from 74% at level 2 to 43% at levels 4 and 5a. For weakly stable conditions ($0 < Ri_b \leq 0.05$) the observed median differences at the upper levels are still positive but increase with height from 11% at level 2 to 31% at level 5a. With increasing stability, the observed median differences at the upper levels remain positive and generally
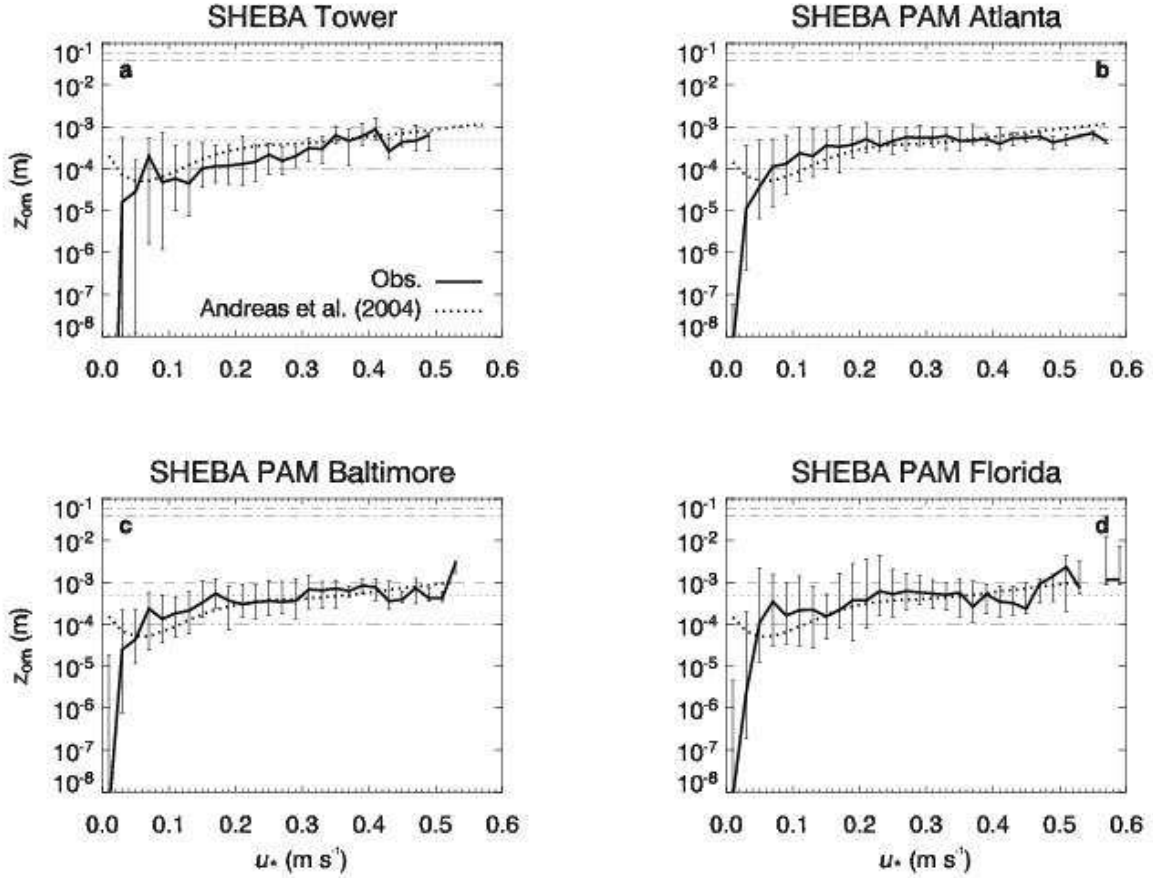
FIG. 8. Median observed roughness lengths for momentum z_{om} (bold solid lines) for 0.02 m s^{-1} bins of friction velocity u_* for surface temperatures colder than -4°C at the (a) 20-m tower and the PAM stations (b) Atlanta, (c) Baltimore, and (d) Florida. The thin vertical lines represent the interquartile range, i.e. the difference between the 75th and 25th percentiles, for each bin. Also shown are the roughness lengths from Andreas et al. (2004) as given by Eq. (15) (bold dotted lines) and the roughness lengths used in the ARCSyM (thin dot-dash lines), ECMWF (thin dashed lines), CCSM (thin dotted lines), and GFS (thin triple dot-dash lines) algorithms.

become higher in magnitude.

Also listed in Table 3 are the median SH fluxes calculated by the four model algorithms used in this study at the lowest level of the tower as well as the median differences at the higher levels relative to the median flux at the lowest level. In general, the model algorithms produce lower fluxes under all regimes. There are a few exceptions: ARCSyM under unstable conditions ($Ri_b \leq 0$), CCSM and ECMWF at levels 4 and 5a in the weakly stable regime ($0 < Ri_b \leq 0.05$), CCSM at all levels in the transitional regime ($0.05 < Ri_b \leq 0.25$), and GFS at level 5a in the very stable regime ($Ri_b > 0.25$).

5. OBSERVED ROUGHNESS LENGTHS DURING THE SHEBA EXPERIMENT

In order to evaluate the validity of the roughness lengths used by the model algorithms compared here, the roughness lengths were derived from the observed turbulent fluxes at the 20-m tower and the PAM stations during the SHEBA experiment. This was done by finding the turbulent parameters u_*, θ_*, and q_*:

$$u_* = \left(\frac{\tau}{\rho_a}\right)^{1/2} \tag{9}$$
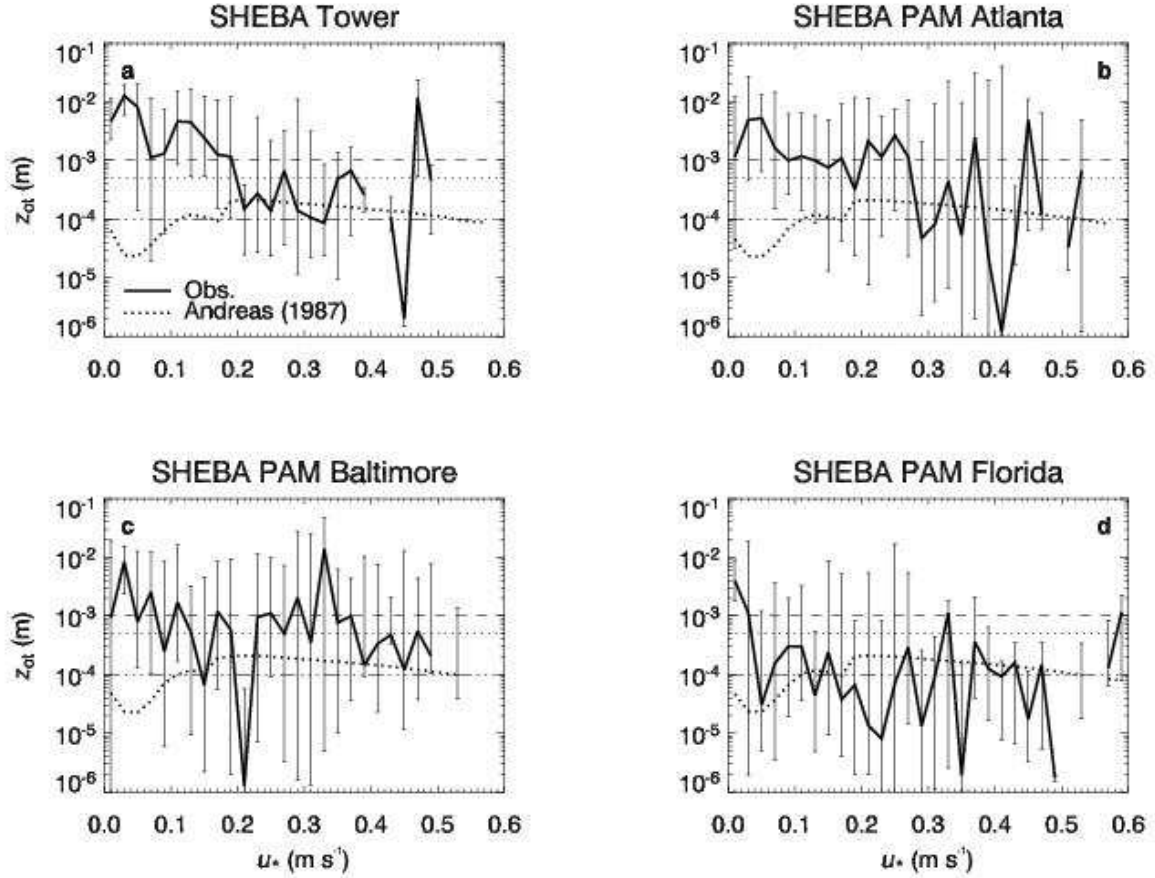
$$\theta_* = -\frac{H_s}{\rho_a c_p u_*} \tag{10}$$

FIG. 9. Same as in Fig. 8 except for the roughness length for heat z_{ot}. Also shown are the roughness lengths from Andreas (1987) (bold dotted lines) as given by Eq. (16).

$$q_* = - \frac{H_l}{\rho_a L_s u_*} \tag{11}$$

Thus, the roughness lengths for momentum, heat, and moisture are derived from the wind, potential temperature, and specific humidity profiles according to Monin-Obukhov similarity theory. In general form, these are:

$$U(z) = \frac{u_*}{k} [\ln(\frac{z}{z_{om}}) - \psi_m] \tag{12}$$

$$\theta(z) - \theta_s = \frac{\theta_*}{k} [\ln(\frac{z}{z_{ot}}) - \psi_t] \tag{13}$$

$$q(z) - q_s = \frac{q_*}{k} [\ln(\frac{z}{z_{oq}}) - \psi_t] \tag{14}$$

where $U(z)$, $\theta(z)$, and $q(z)$ are the wind speed, potential temperature, and specific humidity respectively at the height of observation. Values for z_{om}, z_{ot}, and z_{oq} that were larger than 0.1 m as well as values for z_{ot} and z_{oq} that were smalller

than the mean free path of an air molecule (7 × 10^{-8} m) were excluded. Shown here are only z_{om} and z_{ot}, since LH flux which was recovered very infrequently was only observed at the tower.

Fig. 7 shows the median roughness length for momentum z_{om} for 0.02 m s^{-1} bins of friction velocity u_* when the surface temperature was colder than -4°C. Unlike the constants used in all four of the model algorithms used in this study, z_{om} appears to increase exponentially towards the value used in the ECMWF algorithm (0.001 m) for $u_* \geq 0.05$ m s^{-1} at all of the sites. For smaller u_*, z_{om} decreases very rapidly. These small u_* correspond to very weak winds. It is believed that sonic anemometers do not measure the turbulent fluxes very well under these conditions, so the roughness lengths obtained under these conditions are suspect.

Also shown are the roughness lengths obtained from Andreas et al. (2004) (bold dotted lines):

	b_0	b_1	b_2
$Re_* \leq 0.135$	1.250	0.149	0.317
$0.135 < Re_* < 2.5$	0	-0.550	-0.565
$0.135 < Re_* < 2.5$	0	0	-0.183

$$z_{om} = \frac{0.135\,\nu}{u_*} + \frac{0.035\,u_*^2}{g}$$

$$\{1 + A\exp[-(\frac{u_* - 0.18}{0.10})^2\,]\} \quad (15)$$

where ν is the viscosity of air and A is a coefficient that is tuned to a particular location. For SHEBA, $A = 1$. This formulation is very similar to that used over the ocean which includes an aerodynamically smooth regime (the first term on the right) and a saltation regime. The Andreas et al. (2004) scheme seems to agree very well with the observed roughness lengths.

Fig. 8 presents the median roughness lengths for heat z_{ot} for bins of u_*. Unlike z_{om}, there does not seem to be much of a trend in z_{ot}. Also shown are the roughness lengths obtained from Andreas(1987):

$$z_{ot} = z_{om}\,[b_0 + b_1\,(\ln Re_*) + b_1\,(\ln Re_*)^2] \quad (16)$$

where z_{om} is that obtained from Eq. (15), Re_* is the Roughness Reynolds number $= u_* z_{om} / \nu$ and b_0, b_1, and b_2 are coefficients that vary with Re_* as given in Table 4. There is some slight agreement between these roughness lengths and observed for $u_* \geq 0.2$ m s^{-1}.

6. DISCUSSION AND CONCLUSIONS

A comparison with observations made during the Surface Heat Budget of the Arctic Ocean experiment of the turbulent fluxes produced by algorithms from four climate and numerical weather prediction models, the Community Climate System Model (CCSM), the European Centre for Medium-Range Weather Forecasts (ECMWF) model, the Arctic Regional Climate System Model (ARCSyM), and the National Center for Environmental Prediction (NCEP) Global Forecasting System (GFS) model, has revealed that there are some significant differences between the algorithm results and observed. In particular, all of the algorithms underestimate SH flux and overestimate LH flux during the summer. Also, there are some significant differences between some results by particular algorithms and observed. For instance, ARCSyM overestimates wind stress under unstable conditions ($Ri_b < 0$) , and GFS produces much lower SH fluxes for the transitional and very stable regimes ($Ri_b \geq 0.05$). The former is most likely due to the large roughness lengths used in ARCSyM (see Table 1), while the latter might be due to the stability terms used in GFS (see Table 2). Lowering the roughness lengths in ARCSyM lowers the median wind stress at the lowest level for unstable conditions in winter by 76%. Changing the stability terms in GFS to those used in CCSM and ECMWF for stable conditions increases the SH fluxes produced by this algorithm especially in the very stable regime where there is an almost 50% increase in SH flux.

There is also a large disagreement under most conditions between what the algorithms produce using observations from the levels above the first level at the 20-m tower and observations of the direct fluxes measured. Observed SH fluxes in the winter are consistently higher under stable conditions with the magnitude of the median differences relative to the median flux at level 1 increasing with more significant stability. However, the model algorithms generally produce lower fluxes at the upper levels than at the lowest level with exceptions for CCSM and ECMWF at the highest levels for the weakly stable regime, GFS at the highest level for the very stable regime, and CCSM at all levels in the transitional regime. It is possible that under these stable conditions Monin-Obukhov similarity theory which is widely used in modeling is no longer valid at these upper levels and should be replaced by local or z-less scaling (Mahrt 1999).

Finally, an analysis of the roughness lengths for momentum reveals that it is exponential in nature for $u_* \geq 0.05$ m s^{-1} similar in nature to that produced by the Andreas et al. (2004) sheme. There is no trend to the roughness length for heat and most likely can continue to be considered a constant in models at about 0.0001 m as is used in GFS for surface temperatures colder than -4°C. This is consistent with what was found by Andreas et al. (2004).

REFERENCES

Andreas, E. L., 1987: A theory for the scalar roughness and the scalar transfer coefficients over snow and sea ice. *Bound.-Layer Meteor.*, **38**, 159-184.

Andreas, E. L., R. E. Jordan, P. S. Guest, P. O. G. Persson, A. A. Grachev, and C. W. Fairall, 2004: Roughness lengths over snow. Preprint CD-ROM, *18th Conf. on Hydrology*, Amer. Meteor. Soc., Seattle, WA, JP4.31.

Bitz, C. M., and W. H. Lipscomb, 1999: An energy-conserving thermodynamic model of sea ice. *J. Geophys. Res.*, **104**, 15 669-15 677.

Curry, J. A., J. L. Schramm, E. E. Ebert, 1995: Sea ice-albedo climate feedback mechanism. *J. Climate*, **8**, 240-247.

Gates, W. L., and Coauthors, 1996: Climate models—Evaluation. *Climate Change 1995*, J. T. Houghton, L. G. Meira Filho, B. A. Callander, N. Harris, A. Kattenberg, and K. Maskell, Eds., Cambridge University Press, 233-284.

Houghton, J. T., G. J. Jenkins, and J. J. Ephraums, Eds., 1990: *Climate Change: The IPCC Scientific Assessment*. Cambridge University Press, 364 pp.

Howell, J. F., and J. Sun, 1999: Surface-layer fluxes in stable conditions. *Bound.-Layer Meteor.*, **90**, 495-520.

Kiehl, J. T., and P .R. Gent, 2004: The Community Climate System Model, version two. *J. Climate*, in press.

Mahrt, L., 1999: Stratified atmospheric boundary layers. *Bound.-Layer Meteor.*, **90**, 375-396.

Mahrt, L., J. Sun, W. Blumen, T. Delany, and S. Oncley, 1998: Nocturnal boundary-layer regimes. *Bound.-Layer Meteor.*, **88**, 255-278.

Persson, P. O. G., C. W. Fairall, E. L. Andreas, P. S. Guest, and D. K. Perovich, 2002: Measurements near the Atmospheric Surface Flux Group tower at SHEBA: Near-surface conditions and surface energy budget. *J. Geophys. Res.*, **107**, doi: 10.1029/2000JC000705.

Randall, D. A., and Coauthors, 1998: Status of and outlook for large-scale modeling of atmosphere-ice-ocean interactions in the Arctic. *Bull. Amer. Meteor. Soc.*, **79**, 197-219.

Stocker, T. F., and Coauthors, 2001: Physical climate processes and feedbacks. *IPCC Climate Change 2001: The Scientific Basis*, J. T. Houghton and Co-editors, Eds., Cambridge University Press, 417-470.